

Multiphoton Transitions in a Superconducting Flux Qubit

Shiro Saito[†], Hirotaka Tanaka, Kouichi Semba, and Hideaki Takayanagi

Abstract

We have observed multiphoton transitions between two macroscopic quantum-mechanical superposition states of a superconducting flux quantum bit (qubit) consisting of a superconducting loop with three Josephson junctions. Two persistent currents circulating in opposite directions in the loop are macroscopically distinct states. Resonant peaks and dips of up to three-photon transitions were observed in spectroscopic measurements when the system was irradiated with a strong radio frequency (RF) photon field. The widths of the multiphoton absorption dips shown to scale with the Bessel functions are in agreement with theoretical predictions derived from Bloch equations and the dressed-atom description. From this analysis, we obtained the relaxation and dephasing time of the qubit, which are measures of the qubit's quality and its environment. This information should prove useful for designing and optimizing qubits in the future.

1. Introduction

Quantum state engineering has become one of the most attractive fields in modern physics. Nuclear magnetic resonance techniques in atomic and molecular physics have been studied enthusiastically in relation to quantum computation and communication [1]. In principle, any quantum two-state system has the potential to be applied to a quantum bit (qubit). Of the many candidates that may enable us to achieve quantum computation, superconducting qubits based on Josephson junctions have been gaining importance. Solid-state qubits such as semiconductor qubits or superconducting qubits have the distinct merit of scalability due to the mature state of nanometer-scale fabrication technology. Furthermore, their coherence times have been greatly improved in recent years [2]. There are three types of superconducting qubit. With the first, the charge degree of freedom of Cooper pairs is used to induce coherent quantum oscillations between two charge states of a Cooper pair box [2],

[3]. The second type, known as the Josephson phase qubit, consists of a circuit with a single relatively large Josephson junction, which is current-biased close to its critical current [4]. The third type is the flux qubit where three Josephson junctions are arranged in a superconducting loop and threaded by an externally applied magnetic flux [5]. Several qubit operations have been reported with this system [6]. The device could also be prepared in a quantum superposition of the two states carrying opposite macroscopic persistent currents [7]. From the viewpoint of macroscopic quantum phenomena, it is interesting that macroscopically distinguishable states, such as a persistent current, form the superposition states.

The energy scale of quantum circuits containing Josephson junctions is in the microwave regime. This property was demonstrated in the current-voltage characteristics of a Josephson junction under microwave irradiation displaying the well-known Shapiro steps [8]. They appear at voltages corresponding to integer multiples of the applied microwave energy. With this phenomenon, the superconductor phase difference at the junction, which is a macroscopic degree of freedom, can be treated as a classical degree of freedom moving in the Josephson

[†] NTT Basic Research Laboratories
Atsugi-shi, 243-0198 Japan
E-mail: s-saito@will.brl.ntt.co.jp

potential in phase space. In contrast, the quantum-mechanical behavior of the macroscopic phase difference was demonstrated using one-photon absorption processes between quantized energy levels within a single Josephson potential well [9]. Recently, Wallraff *et al.* presented experimental evidence of multiphoton absorption between quantized energy levels within a single potential well formed by a large current-biased Josephson junction [10]. In this paper, we report the first observation of multiphoton transitions between superposition states of a *macroscopically distinct state* [11], which are formed in the double-well potential system of a superconducting flux qubit [12].

2. Experiment

2.1 Sample fabrication

Figure 1(a) shows a scanning electron microscope image of a superconducting flux qubit system. The inner loop with three Josephson junctions constitutes the flux qubit and the outer loop with two junctions is a dc-SQUID (superconducting quantum interference device) acting as a qubit state detector. They are spa-

tially separated but magnetically coupled (mutual inductance $M \approx 7 \text{ pH}$). The area of the qubit loop is $5.1 \times 5.3 \mu\text{m}^2$ and the dc-SQUID is $7.3 \times 7.7 \mu\text{m}^2$. The qubit contains two identical Josephson junctions and one that is $\beta (=0.7)$ times smaller. They have junction areas of 100×300 and $100 \times 210 \text{ nm}^2$, respectively. The Josephson energy $E_J = \hbar I_c/2e$ of the two identical junctions and the energy splitting $\hbar\Delta$ at the degeneracy point were 340 and 0.54 GHz, respectively, as estimated from spectroscopy measurements. Here, I_c is the critical current of the junction and e is the electron charge. The qubit system is made of aluminum and is contacted by on-chip gold leads and pads. A 260- μm -wide on-chip Au-strip line induces oscillating magnetic fields in the qubit loop. The distance between the qubit and the edge of the strip line is 20 μm . The 100-nm-thick strip line and the leads and pads were manufactured on a silicon wafer with 1 μm of SiO_2 by e-beam lithography and the liftoff technique. We then fabricated the qubit system using e-beam lithography and the standard shadow evaporation technique [13]. Two successive aluminum layers (40 and 50 nm) were deposited on the substrate. After depositing the first

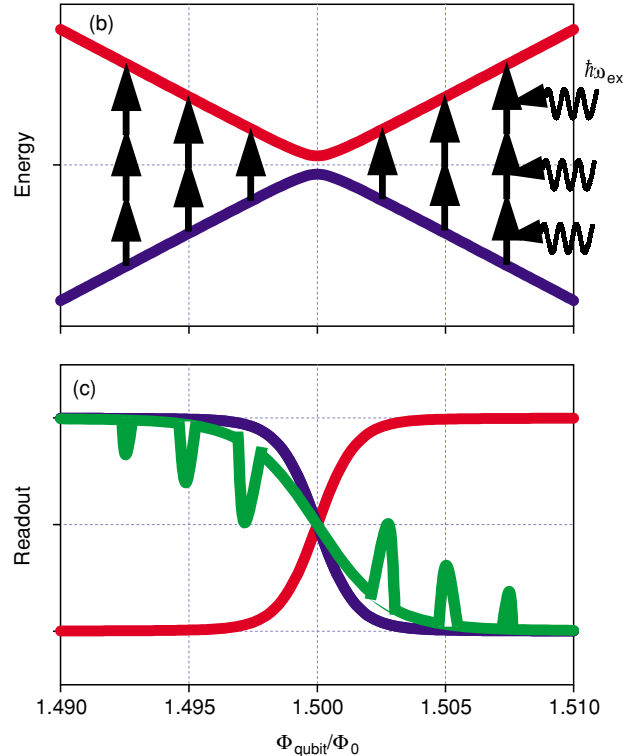
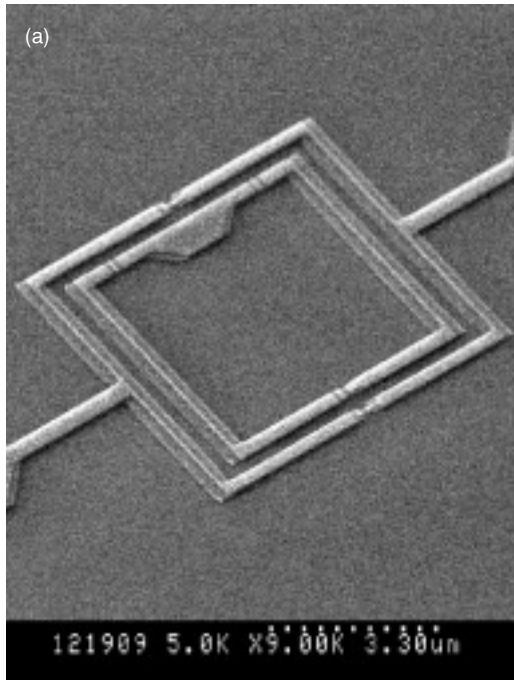


Fig. 1. (a) Scanning electron microscope image of a superconducting flux qubit system. (b) Schematic illustration of qubit energy levels as a function of the applied flux around $\Phi_{\text{qubit}}/\Phi_0 = 1.5$. The blue and red curves represent the ground and first excited states of the qubit. The upward pointing arrows indicate multiphoton absorption processes. (c) Schematic drawing of the qubit readout at around $\Phi_{\text{qubit}}/\Phi_0 = 1.5$. The green curve represents the average thermal readout between the ground (blue curve) and the first excited state (red curve) under microwave irradiation.

layer, we oxidized it with 1 mTorr of pure oxygen for 2 minutes. The double evaporation direction is shifted by $\pm 17^\circ$ to create Al overlaps forming Josephson junctions.

2.2 Superconducting flux qubit

By carefully designing the junction parameters [5]-[7], we can make the inner loop behave as an effective quantum two-state system. In fact, the qubit readout changes greatly with the qubit design, ranging from the purely classical regime to the quantum regime [14]. It is described by the Hamiltonian $\hat{H}_{qb} = \frac{\hbar}{2}(\varepsilon_0\hat{\sigma}_z + \Delta\hat{\sigma}_x)$, where $\hat{\sigma}_{x,z}$ are the Pauli spin operators. Two eigenstates of $\hat{\sigma}_z$ are localized states $|\downarrow\rangle$ corresponding to the persistent clockwise current of the qubit and $|\uparrow\rangle$ corresponding to its persistent anticlockwise current. The energy eigenstates $|0\rangle$ and $|1\rangle$ of \hat{H}_{qb} show an energy anticrossing with energy gap $\hbar\Delta$ at the degeneracy point. An externally applied static magnetic flux Φ_{qubit} generates the energy bias $\hbar\varepsilon_0 = I_p\Phi_0(\Phi_{qubit}/\Phi_0 - f_{op})$ between the two localized states, where $\Phi_0 = h/2e$ is the flux quantum, $I_p = I_C\sqrt{1-(1/2\beta)^2}$ is the persistent current of the qubit, and f_{op} is the qubit operating point, which is a half integer. The effective energy gap in the biased qubit is $\hbar\Delta_b = \hbar\sqrt{\varepsilon_0^2 + \Delta^2}$. The qubit dynamics is controlled by a time-dependent RF field $s(t) = s\cos\omega_{ex}t$ with amplitude s and frequency ω_{ex} provided by an on-chip RF-line. This leads to an additional term in the Hamiltonian $\hat{H}_{RF}(t) = -\frac{\hbar}{2}s(t)\hat{\sigma}_z$.

Figure 1(b) shows a schematic energy diagram of the qubit as a function of Φ_{qubit}/Φ_0 . The blue and red curves represent the ground state $|0\rangle$ and the first excited state $|1\rangle$, respectively. They show the energy anticrossing with energy gap $\hbar\Delta$ at the degeneracy point $\Phi_{qubit}/\Phi_0 = 1.5$. The arrows schematically describe the processes by which the qubit absorbs the RF photon when the effective energy gap $\hbar\Delta_b$ matches an integer multiple of the RF photon energy $n\hbar\omega_{ex}$. If Δ is zero, $\hat{H}_{qb} + \hat{H}_{RF}(t)$ has only diagonal terms. In this case, the RF field cannot excite the qubit from the ground state to any excited state. A non-zero Δ is therefore a prerequisite for a spectroscopic experiment. In other words, resonant peaks and dips in the qubit signals are direct evidence for the coherent superposition of the macroscopically distinct states and for the mul-

tiphoton transitions that occur between them.

2.3 Qubit readout

When the external flux Φ_{qubit}/Φ_0 diverges slightly from half integers, the observable difference between the qubit states $|0\rangle$ and $|1\rangle$ is the direction of the flux induced by the qubit circulation current. To measure the flux, we used the current-voltage (*I-V*) characteristics of a dc-SQUID, which worked as a highly sensitive flux detector. The switching current, where the voltage across the dc-SQUID jumps from zero to a finite value in the *I-V* characteristics, depends on the magnetic flux piercing the dc-SQUID. We can therefore detect the qubit states by measuring the switching currents of the dc-SQUID. The switching current was typically obtained by averaging the values of 500 measurements. **Figure 1(c)** shows schematic readout curves of the qubit corresponding to $|0\rangle$ (blue curve) and $|1\rangle$ (red curve). Because the measurements were carried out in a dilution refrigerator at a temperature of 30 mK and were averaged, we observed the thermal average between them (like the green curve, which is calculated) [15]. With the microwave irradiation, we also observed resonant peaks and dips due to the multiphoton absorption. The bias voltage needed to obtain the *I-V* characteristics had a triangular waveform and was fed through large bias resistors of 1 M Ω to achieve a current-bias measurement. The sweep rate of the current was set at 120 μ A/s and the frequency of the wave was 310 Hz. The RF line used to apply microwaves contained three attenuators in the input line: 30 dB at room temperature, 10 dB at 4.2 K, and 10 dB at the base temperature. We fabricated an on-chip strip line to achieve strong coupling between the qubit and the RF line.

To achieve a good readout resolution, we chose the operating point f_{op} to be $\Phi_{qubit}/\Phi_0 = 1.5$. **Figure 2** shows the signal-to-noise (S/N) ratio $\Delta I_{qb}/I_{std}$ (red curve) and average switching current I_{sw} (blue curve) as a function of the applied flux through the qubit loop, where I_{std} denotes the standard deviation of the SQUID switching currents over 150 events, which may be considered to be the noise level in the qubit readout. The qubit signal amplitude ΔI_{qb} should be proportional to the flux derivative of I_{sw} , which means that we can estimate ΔI_{qb} by using the signal amplitude ΔI_{qb0} at $\Phi_{qubit}/\Phi_0 = 1.5$ (see **Fig. 3(a)**). In the experiments, the qubit signal appeared when Φ_{qubit}/Φ_0 was a half-integer and the two arrows in Fig. 2 indicate the S/N ratio at $\Phi_{qubit}/\Phi_0 = 0.5$ and 1.5. Hence we chose the operating point to be $\Phi_{qubit}/\Phi_0 = 1.5$ to achieve a higher readout resolution.

3. Results and discussion

3.1 Experimental results

Figure 3(a) shows the qubit signal δI_{sw} as a function of the external flux Φ_{qubit} at $\Phi_{\text{qubit}}/\Phi_0 \approx 1.5$, which is

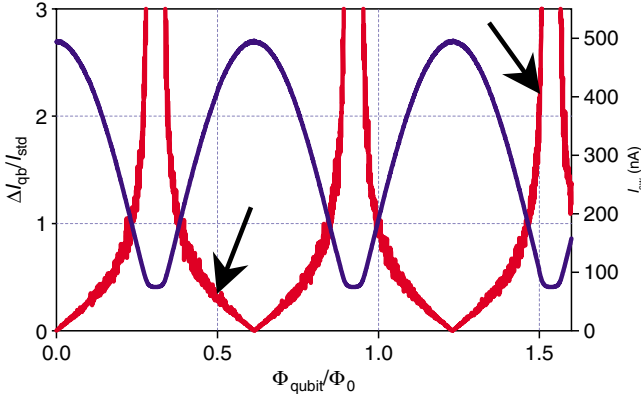


Fig. 2. Signal-to-noise (S/N) ratio $\Delta I_{\text{qb}}/I_{\text{std}}$ and the switching current of the dc-SQUID I_{sw} as a function of applied flux through the qubit loop. The two arrows show the S/N ratio at the qubit operating points $\Phi_{\text{qubit}}/\Phi_0 = 0.5$ and 1.5 .

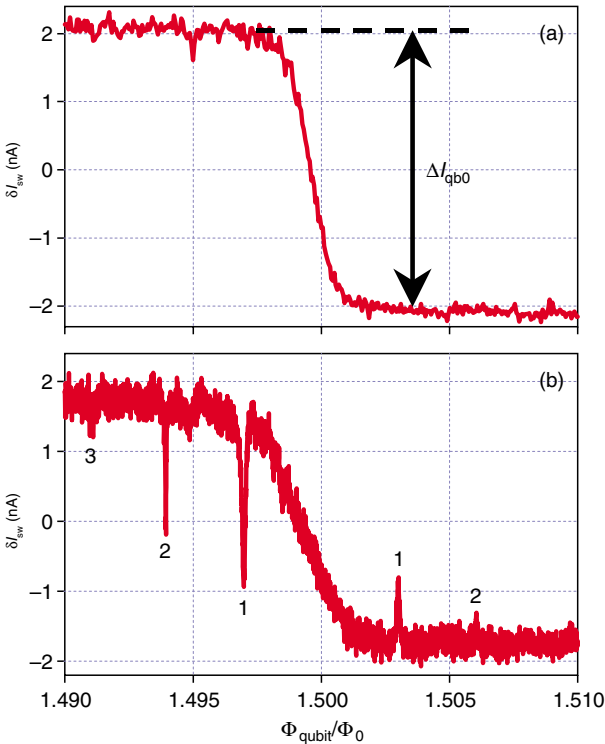


Fig. 3. Applied magnetic flux dependence of the qubit signal δI_{sw} . (a) Without microwave irradiation. The data were obtained after averaging 2000 measurements. (b) With microwave irradiation. The data were obtained after averaging 500 measurements. The microwave power and frequency were 5 dBm at the generator and 9.1 GHz, respectively.

derived by subtracting the sinusoidal background switching current from the SQUID switching current I_{sw} . It shows a change in the thermal average persistent current of the qubit [7]. We obtained a sample temperature of 65 mK from a numerical fit to the data by using the qubit parameters E_J and Δ , which we derived from spectroscopy measurements. **Figure 3(b)** shows the Φ_{qubit} dependence of the qubit signal under microwave irradiation. The distinct resonant peaks and dips are attributed to situations where the energy separation of the two qubit states $\hbar\Delta_b$ matches an integer multiple of the RF photon energy $n\hbar\omega_{\text{ex}}$. We have detected up to three resonant peaks and dips for various fixed RF frequencies. The half width at half maximum (HWHM_n) and the normalized amplitude A_n of the dips are shown in **Figs. 4(a)** and **(b)** for various microwave amplitudes I_{RF} for $n = 1, 2, 3$, which is defined by $I_{\text{RF}} = 10^{P_{\text{RF}}/20}$. Here, P_{RF} (dBm) is the microwave power at the signal generator. We derived the HWHM_n and A_n by fitting the $\Phi_{\text{qubit}}/\Phi_0$ dependence of δI_{sw} around the resonant dips (see Fig. 3(b)) using a Lorentzian. The A_n values are normal-

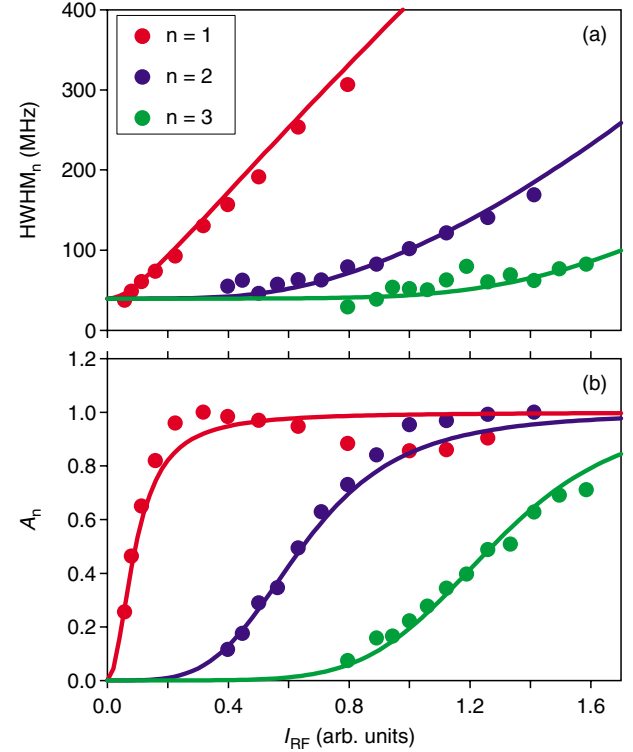


Fig. 4. Half width at half maximum (a) and normalized amplitude (b) of the resonant dips as functions of the microwave amplitude I_{RF} . The solid curves represent theoretical fits obtained by Bloch equations combined with the dressed-atom approach.

ized by the full amplitude of the dips (3 nA). The HWHM_n carries important information about the dephasing and relaxation processes caused by the interaction with the environment. To calculate the line shape of the one-photon absorption dip, we used phenomenological Bloch equations. To describe the strong driving region and the n -th dip, we replaced the single-photon Rabi frequency ω_1 in the Bloch equations with the corresponding multi-photon frequency derived from the theory of the dressed-atom approach [16]. This substitution has been verified by numerical simulations [17]. This method yields results that are in excellent agreement with experimentally obtained ones, as seen in Fig. 4.

3.2 Bloch equations

The Bloch equations describe the dynamics of a spin-1/2 in a constant field in the z -direction and a time-dependent field perpendicular to it [18]. With the flux qubit, the constant field represents the effective energy gap $\hbar\Delta_b$, namely the Larmor frequency and the time-dependent field comes from the applied microwave, which causes Rabi oscillation. To maintain the analogy between the spin-1/2 and the flux qubit, we write the Hamiltonian in terms of the energy eigenstates [19] and obtain

$$\hat{H} = \frac{\hbar}{2} \left(\left\{ \Delta_b - \frac{\varepsilon_0}{\Delta_b} s(t) \right\} \hat{\sigma}_z + \frac{\Delta}{\Delta_b} s(t) \hat{\sigma}_x \right). \quad (1)$$

The second term of the Hamiltonian leads to a non-adiabatic periodic variation in the Larmor frequency. When $\frac{\varepsilon_0}{\Delta_b} s \approx \Delta_b$, the Rabi frequency is decreased. However, we can disregard this term under the usual experimental condition, $\frac{\varepsilon_0}{\Delta_b} s < \Delta_b$. We have confirmed this by numerical simulations. If we use the rotating-wave approximation, the motion of the qubit spin $\langle \hat{\sigma}(t) \rangle$ in the laboratory frame can be described by the Bloch equations

$$\begin{aligned} \frac{d\langle \hat{\sigma}_x(t) \rangle}{dt} &= \left[\gamma \langle \hat{\sigma}(t) \rangle \times B(t) \right]_x - \frac{\langle \hat{\sigma}_x(t) \rangle}{T_\phi}, \\ \frac{d\langle \hat{\sigma}_y(t) \rangle}{dt} &= \left[\gamma \langle \hat{\sigma}(t) \rangle \times B(t) \right]_y - \frac{\langle \hat{\sigma}_y(t) \rangle}{T_\phi}, \\ \frac{d\langle \hat{\sigma}_z(t) \rangle}{dt} &= \left[\gamma \langle \hat{\sigma}(t) \rangle \times B(t) \right]_z - \frac{\langle \hat{\sigma}_z(t) \rangle - \sigma_0}{T_r}. \end{aligned} \quad (2)$$

Here, $\gamma B(t) = -\frac{\hbar}{2}(\omega_1 \cos \omega_{\text{ex}} t, \omega_1 \sin \omega_{\text{ex}} t, \Delta_b)$, σ_0

is the thermal equilibrium value of $\langle \hat{\sigma}_z(t) \rangle$, T_r and T_ϕ are the relaxation and dephasing times, and $\omega_1 = \frac{s\Delta}{2\Delta_b}$ is the Rabi frequency of the one-photon absorption process. The steady-state solutions of Eqs. (2) can be

obtained in the rotating frame by setting $\frac{d\langle \hat{\sigma}_i(t) \rangle}{dt} = 0$,

where $i = x, y, z$. Our dc-SQUID measures the flux produced by the qubit circulating current. This means that the readout corresponds to the z -component of the qubit spin $\langle \hat{\sigma}(t) \rangle$. Hence we are interested in $\langle \hat{\sigma}_z(t) \rangle$ of the steady state, which is given by

$$\langle \hat{\sigma}_z \rangle = \left(1 - \frac{\omega_1^2 T_r T_\phi}{1 + (\Delta\omega T_\phi)^2 + \omega_1^2 T_r T_\phi} \right) \sigma_0, \quad (3)$$

where $\Delta\omega \equiv \Delta_b - \omega_{\text{ex}}$. In Eq. (3), a resonant dip due to one photon with a Lorentzian line shape appears at around $\omega_{\text{ex}} \approx \Delta_b$. The HWHM₁ and the amplitude A_1 of the resonant dip are

$$\begin{aligned} \text{HWHM}_1 &= \sqrt{\left(\frac{1}{T_\phi} \right)^2 + \omega_1^2 \left(\frac{T_r}{T_\phi} \right)^2}, \\ A_1 &= \frac{\omega_1^2 T_r T_\phi}{1 + \omega_1^2 T_r T_\phi} \sigma_0. \end{aligned} \quad (4)$$

3.3 Dressed-atom approach

To describe the regime of strong driving and n -photon absorption processes, we apply the dressed-atom approach to the flux qubit. The Hamiltonian is given by

$$\hat{H} = \frac{\hbar}{2} (\varepsilon_0 \hat{\sigma}_z + \Delta \hat{\sigma}_x) + \hbar \omega_{\text{ex}} a^\dagger a + g \hat{\sigma}_z (a + a^\dagger),$$

where a and a^\dagger are the annihilation and creation operators for a field mode with angular frequency ω_{ex} and g is a coupling constant between the qubit and the field. The first term represents the qubit Hamiltonian in the basis of the localized state $|\downarrow\rangle$ and $|\uparrow\rangle$. The Hamiltonian can be explicitly diagonalized when $\Delta = 0$. The eigenstates are given by $|\uparrow(\downarrow); N\rangle_{\text{dressed}} = \exp[-(+g(a^\dagger - a)/\hbar\omega_{\text{ex}})] |\uparrow(\downarrow)\rangle |N\rangle$ and their eigen-energies are $E_N^{(\uparrow\downarrow)} = N\hbar\omega_{\text{ex}} - g^2/\hbar\omega_{\text{ex}} + (-)\frac{1}{2}\hbar\varepsilon_0$, where $|N\rangle$ are eigenstates of $\hbar\omega_{\text{ex}} a^\dagger a$. For $\Delta \ll \varepsilon_0$, first-order perturbation theory in the qubit Hamiltonian yields a term that is linear in Δ and when $n\hbar\omega_{\text{ex}} \approx \hbar\Delta_b$, the two dressed states show anticross-

ing due to off-diagonal coupling $\frac{\hbar\Delta}{2} J_n(\alpha)$. Here, $J_n(\alpha)$ is the n -th order Bessel function of the first kind and $\alpha \equiv 4g\sqrt{\langle N \rangle}/\hbar\omega_{\text{ex}}$ is the scaled amplitude of the driving field. If we prepare a localized initial state, Rabi oscillations occur with frequency $\omega_n = |\Delta|J_n(\alpha)$ [20].

To analyze the HWHM _{n} and A_n of the resonant dips, we substituted ω_n for ω_l in Eqs. (4). We used T_{r1} , T_{r2} , T_{r3} , $T_{\phi n} = T_\phi$, and c as fitting parameters. Here, T_m and $T_{\phi n}$ are the relaxation and dephasing times related to the n -th photon absorption process. We defined a coupling constant c as $cI_{\text{RF}} = \alpha$. We found excellent agreement between the calculated and experimental data for both HWHM _{n} and A_n (see Fig. 4). We obtained $T_{r1} = 31$ ns, $T_{r2} = 84$ ns, $T_{r3} = 430$ ns, $T_\phi = 4.0$ ns, and $c = 0.55$ from the fitting at a microwave frequency of 3.8 GHz. We have obtained similar results for $\omega_{\text{ex}}/2\pi = 9.1$ and 11.4 GHz (not shown). It should be noted that the relaxation and dephasing times T_m and T_ϕ do not depend on the frequency of the corresponding multiphoton transition for a pure structureless ohmic environment (see also Eqs. (2)). This is no longer the case for a more complicated structured harmonic environment [21] as is present in our device. Here, the plasmon frequency of the dc-SQUID provides an additional energy scale of the environment. Nevertheless, the global physics is captured by our simplified model.

4. Conclusion

In conclusion, we reported on measurements of macroscopic superconducting circuits that reveal their quantum-mechanical behavior at low temperature. We identified multiphoton transition processes in the qubit and found that the width of the n -photon resonance scales with the n -th Bessel function with its argument given by the ratio of the driving-field strength to the frequency of the photons. We also obtained the relaxation and dephasing times of the qubit, which are measures of the qubit quality and its environment. This information should be useful when designing and optimizing qubits in the future.

5. Acknowledgments

We thank M. Thorwart (Heinrich-Heine-Universität Düsseldorf) for theoretical analysis; M. Ueda (NTT, Tokyo Institute of Technology), H. Nakano (NTT), J. E. Mooij (Delft University of Technology), C. J. P. M. Harmans (Delft University of Technolo-

gy), M. Grifoni (Universität Regensburg), I. Chiorescu (Michigan State University), Y. Nakamura (NEC Fundamental Research Laboratories), and D. Vion (CEA Saclay) for useful discussions; and T. Kutsuzawa (NTT, Tokyo University of Science) for experimental help. This work has been supported by the CREST project of the Japan Science and Technology Agency (JST).

References

- [1] M. A. Nielsen and I. L. Chuang, "Quantum Computation and Quantum Information," pp. 324-343, Cambridge University Press, Cambridge, 2000.
- [2] D. Vion, A. Aassime, A. Cottet, P. Joyez, H. Pothier, C. Urbina, D. Esteve, and M. H. Devoret, "Manipulating the Quantum State of an Electrical Circuit," *Science*, Vol. 296, No. 5569, pp. 886-889, 2002.
- [3] Y. Nakamura, Y. A. Pashkin, and J. S. Tsai, "Coherent Control of Macroscopic Quantum States in a Single-Cooper-pair Box," *Nature*, Vol. 398, No. 6730, pp. 786-788, 1999.
- [4] Y. Yu, S. Han, X. Chu, S.-I. Chu, and Z. Wang, "Coherent Temporal Oscillations of Macroscopic Quantum States in a Josephson Junction," *Science*, Vol. 296, No. 5569, pp. 889-892, 2002; J. M. Martinis, S. Nam, J. Aumentado, C. Urbina, "Rabi Oscillations in a Large Josephson-Junction Qubit," *Phys. Rev. Lett.*, Vol. 89, No. 11, pp. 117901-1 to 117901-4, 2002.
- [5] J. E. Mooij, T. P. Orlando, L. Levitov, L. Tian, C. H. van der Wal, and S. Lloyd, "Josephson Persistent-Current Qubit," *Science*, Vol. 285, No. 5430, pp. 1036-1039, 1999.
- [6] I. Chiorescu, Y. Nakamura, C. J. P. M. Harmans, and J. E. Mooij, "Coherent Quantum Dynamics of a Superconducting Flux Qubit," *Science*, Vol. 299, No. 5614, pp. 1869-1871, 2003.
- [7] C. H. van der Wal, A. C. J. ter Haar, F. K. Wilhelm, R. N. Schouten, C. J. P. M. Harmans, T. P. Orlando, S. Lloyd, and J. E. Mooij, "Quantum Superposition of Macroscopic Persistent-Current States," *Science*, Vol. 290, No. 5492, pp. 773-777, 2000.
- [8] S. Shapiro, "Josephson Currents in Superconducting Tunneling: The Effect of Microwaves and Other Observations," *Phys. Rev. Lett.*, Vol. 11, No. 2, pp. 80-82, 1963; W. C. Danchi, F. Habbal, and M. Tinkham, "ac Josephson Effect in Small-area Superconducting Tunnel Junctions at 604 GHz," *Appl. Phys. Lett.*, Vol. 41, No. 9, pp. 883-885, 1982.
- [9] M. H. Devoret, J. M. Martinis, D. Esteve, and J. Clarke, "Resonant Activation from the Zero-Voltage State of a Current-Biased Josephson Junction," *Phys. Rev. Lett.*, Vol. 53, No. 13, pp. 1260-1263, 1984.
- [10] A. Wallraff, T. Duty, A. Lukashenko, and A. V. Ustinov, "Multiphoton Transitions between Energy Levels in a Current-Biased Josephson Tunnel Junction," *Phys. Rev. Lett.*, Vol. 90, No. 3, pp. 037003-1 to 037003-4, 2003.
- [11] A. J. Leggett, "Testing the Limits of Quantum Mechanics: Motivation, State of Play, Prospects," *J. Phys. Condens. Matter*, Vol. 14, No. 15, pp. R415-R451, 2002.
- [12] S. Saito, M. Thorwart, H. Tanaka, M. Ueda, H. Nakano, K. Semba, and H. Takayanagi, "Multiphoton Transitions in a Macroscopic Quantum Two-State System," *Phys. Rev. Lett.*, Vol. 93, No. 3, 037001-1 to 037001-4, 2004.
- [13] G. J. Dolan, "Offset Masks for Lift-Off Photoprocessing," *Appl. Phys. Lett.*, Vol. 31, No. 5, pp. 337-339, 1977.
- [14] H. Takayanagi, H. Tanaka, S. Saito, and H. Nakano, "Observation of Qubit State with a dc-SQUID and Dissipation Effect in the SQUID," *Phys. Scr.*, Vol. T102, pp. 95-102, 2002; S. Saito, H. Tanaka, H. Nakano, M. Ueda, and H. Takayanagi, "Incoherent and Coherent Tunneling of Macroscopic Phase in Flux Qubits," in "Quantum Computing and Quantum Bits in Mesoscopic Systems," edited by A. J. Leggett, B. Ruggiero, and P. Silvestrini, pp. 161-169, Kluwer, New

- York, 2004; H. Nakano, H. Tanaka, S. Saito, K. Semba, H. Takayanagi, and M. Ueda, "A Theoretical Analysis of Flux-Qubit Measurements with a dc-SQUID," cond-mat/0406622.
- [15] H. Tanaka, S. Saito, H. Nakano, K. Semba, M. Ueda, and H. Takayanagi, "Single-Shot Readout of Macroscopic Quantum Superposition State in a Superconducting Flux Qubit," cond-mat/0407299.
- [16] C. Cohen-Tannoudji, J. Dupont-Roc, and G. Grynberg, "Atom-Photon Interaction," pp. 485-488, Wiley, New York, 1992.
- [17] M. C. Goorden and F. K. Wilhelm, "Theoretical Analysis of Continuously Driven Dissipative Solid-State Qubits," Phys. Rev. Vol. B 68, p. 012508, 2003.
- [18] A. Abaragam, "Principles of Nuclear Magnetism," pp. 19-38, Oxford University Press, Hong Kong, 1961.
- [19] M. C. Goorden, "Theory of Josephson Persistent-Current Qubits with Driving and Dissipation," pp. 15-17, Master's Thesis, TU Delft, Delft, 2002.
- [20] Y. Nakamura, Y. A. Pashkin, and J. S. Tsai, "Rabi Oscillations in a Josephson-Junction Charge Two-Level System," Phys. Rev. Lett., Vol. 87, No. 24, pp. 246601-1 to 246601-4, 2001.
- [21] M. Thorwart, E. Paladino, and M. Grifoni, "Dynamics of the Spin-Boson Model with a Structured Environment," Chem. Phys., Vol. 296, Issues 2-3, pp. 333-344, 2004.

**Shiro Saito**

Research Scientist, Superconducting Quantum Physics Research Group, Physical Science Laboratory, NTT Basic Research Laboratories.

He received the B.E., M.E., and Ph.D. degrees in applied physics from the University of Tokyo, Tokyo in 1995, 1997, and 2000, respectively. In 2000, he joined NTT Basic Research Laboratories, Kanagawa, Japan. Since then, he has been studying superconducting flux qubits. His current interests are improving the qubit coherence time and achieving two-qubit entanglement in solid-state qubits. He is a member of the Japan Society of Applied Physics (JSAP) and the Physical Society of Japan (PSJ).

**Hirotaka Tanaka**

Senior Research Scientist, Superconducting Quantum Physics Research Group, Physical Science Laboratory, NTT Basic Research Laboratories.

He received the M.E. degree in electrical and electronic engineering from Tokyo Institute of Technology, Tokyo in 1995. Then he joined NTT Basic Research Laboratories, Kanagawa, Japan. Since then, he has been engaged in the study of quantum device physics. From 1997 to 1998, he worked in NTT Photo-electronics Laboratories to develop nano-scale fabrication devices using fullerene-doped electron beam resist. He studied in Delft University of Technology in the Netherlands from 1998 to 1999. He is also a visiting lecturer at Nagoya University. He is a member of JSAP and PSJ.

**Kouichi Semba**

Group Leader, Superconducting Quantum Physics Research Group, Physical Science Laboratory, NTT Basic Research Laboratories.

He received the B.S. and M.S. degrees in science and a Ph.D. degree in applied physics from the University of Tokyo, Tokyo in 1983, 1985, and 2002, respectively. In 1985, he joined NTT Electrical Communication Laboratories, Ibaraki, Japan. In 1987, he joined NTT Basic Research Laboratories, Tokyo, Japan. Since then, he has been engaged in the study of the physics of high-Tc cuprate superconductors. In 2002-2003, he was a visiting researcher at Delft University of Technology, the Netherlands. His current interests are achieving and controlling entanglement in superconducting qubits. He is a member of PSJ, JSAP, and the American Physical Society (APS).

**Hideaki Takayanagi**

NTT R&D Fellow, Director, NTT Basic Research Laboratories.

He received the B.S., M.S., and Ph.D. degrees in science from the University of Tokyo, Tokyo in 1975, 1977, and 1987, respectively. In 1977, he joined the Electrical Communication Laboratories, Nippon Telegraph and Telephone Public Corporation (now NTT), Tokyo, Japan. Since 1985, he has been working on superconducting quantum device physics. In 2000, he was awarded the Nissan Science Prize. He is also a visiting professor at the University of Tokyo and Tokyo University of Science. He is a member of PSJ, JSAP, and APS.